Letter

Magnetic structure of oxygen-deficient perovskite nickelates with ordered vacancies

Yongjin Shin and James M. Rondinelli*

Department of Materials Science and Engineering, Northwestern University, Evanston, Illinois 60208, USA

(Received 21 April 2022; accepted 3 June 2022; published 30 June 2022)

The oxygen vacancy concentration in $LaNiO_{3-\delta}$ nickelate perovskites affects magnetic interactions and long-range magnetic order through changes in local electronic configurations, crystal field splitting energies, and polyhedral arrangements. Here we use density functional theory calculations to examine the magnetic structure of $LaNiO_{2.5}$ and $LaNiO_{2.75}$ with structural ordered oxygen vacancies (OOV). These OOV phases exhibit columnar arrangements of NiO_4 square planar units, which adopt low-spin Ni^{2+} (d^8) configurations with nominally zero magnetic moment ($S = 0$), interconnected by NiO_6 octahedral units. The magnetic structure of the OOV phases are governed by the flexible charge state of the NiO_6 octahedral units, whose density and connectivity depends on the oxygen vacancy concentration. $LaNiO_{2.5}$ is stable in an insulating A-type antiferromagnetic (AFM) phase derived from octahedral units comprising Ni^{2+} in AFM chains. $LaNiO_{2.75}$ is a narrow-gap insulator with zigzag-type AFM order originating from weakly localized electrons in columnar breathing distortions to the NiO_6 units. Our results suggest that nanoscale OOV phases within single-phase $LaNiO_{3-\delta}$ crystals can account for its reported complex magnetic ground-state structure.

DOI: 10.1103/PhysRevResearch.4.L022069

Rare-earth-element nickelate perovskites, $RNiO_3$, are a family of compounds that exhibits temperature-dependent metal-insulator transitions (MIT) [1–3]. The antiferromagnetic (AFM) ground state at lower temperature is realized by nominal charge disproportionation of Ni^{3+} to Ni^{2+} and Ni^{4+}, associated with rock-salt-type breathing distortions of the corner-connected octahedra [4,5]. The breathing distortion stability depends on the degree of in-phase rotation and tilting distortion, which affects the MIT transition temperature as described in phase diagrams based on R radii or crystallographic tolerance factors [6]. $LaNiO_3$ with its large tolerance factor exhibits $R\bar{3}c$ symmetry, unlike the monoclinic nickelates, which prohibits the breathing distortion [7,8] and accounts for this broad temperature-dependent paramagnetic (PM) metallic behavior.

Formation of oxygen vacancies in $LaNiO_3$ and its impact on the electronic and magnetic structure has drawn renewed interest. First, understanding magnetism of the oxygen-deficient phases is useful for intrepretating the magnetic state of $LaNiO_3$ crystals synthesized with various methods [9–12]. Indeed, along the vacancy-driven transitions in $LaNiO_{3-\delta}$ for δ from 0 to 0.5, a significant change occurs in both electronic (metal-semiconductor-insulator) and magnetic (paramagnetic-ferromagnetic-antiferromagnetic) properties [13,14]. In addition, the end member of this transition, the infinite-layer $RNiO_2$ family, hosts superconductivity [15,16].

The formation of ordered-oxygen vacancies (OOVs) is observed in oxygen-deficient phases, and it transforms NiO_6 octahedra to NiO_4 square planar units as shown in Fig. 1 [14]. The change in coordination number (reduced bandwidth) and electron filling explains the insulating AFM properties of $LaNiO_{2.5}$ found both in experiment and first-principles calculations [10,17–19]. On the other hand, less understanding exists for intermediate oxygen deficiencies between $LaNiO_3$ and $LaNiO_{2.5}$, which have been interpreted as transient states with statistical distributions of oxygen vacancies [14,20], mainly because of limited knowledge of their atomic structures.

Here we perform density functional theory (DFT) calculations to identify and assess stable atomic structures and the corresponding electronic and magnetic properties of $LaNiO_{2.5}$ and $LaNiO_{2.75}$ with OOVs (Fig. 1). We find that out-of-phase rotations of octahedra (like those in the $R\bar{3}c$ perovskite phase) are the most stable distortion occurring in the OOV phases. The *Pnma*-like distortion (with in-phase rotations) energetically competes with them. Furthermore, we show the physical properties are determined by the Ni valence in the NiO_6 octahedral units, as Ni in the square planar unit remains diamagnetic throughout with a low-spin $Ni^{2+}(d^8, S = 0)$ configuration. In $LaNiO_{2.5}$, the octahedral units adopt high-spin Ni^{2+} (d^8, $S = 1$) configurations and form antiferromagnetic chains along the c direction, stabilizing an A-type AFM insulator. In contrast, $LaNiO_{2.75}$ exhibits columnar breathing distortions of octahedra, owing to the internal strain induced by the linking NiO_4 units. This structure connectivity stabilizes charge ordering and a zigzag AFM order with a narrow band gap. Finally, we argue that the magnetic properties observed in $LaNiO_{3-\delta}$ with $0 \leqslant \delta \leqslant 0.5$ can be understood as

*jrondinelli@northwestern.edu

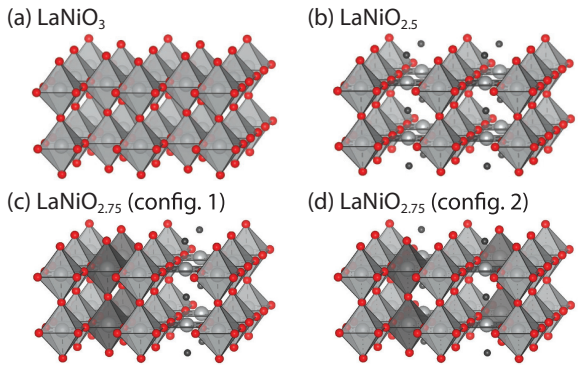

FIG. 1. Structures of vacancy ordered $LaNiO_{3-\delta}$ with varying oxygen vacancy content. (a) $LaNiO_3$, (b) $LaNiO_{2.5}$, (c) $LaNiO_{2.75}$ (config. 1), and (d) $LaNiO_{2.75}$ (config. 2). La atoms are omitted and vacancies are drawn as gray spheres for a better description. Octahedral units with smaller volumes are highlighted with darker shading.

arising from OOVs rather than random oxygen-vacancy distributions.

We used the Vienna *Ab-initio* Simulations Package (VASP) [21,22] to perform our DFT calculations with the Perdew-Burke-Ernzerhof functional (PBE) [23]. Projector-augmented wave (PAW) potentials [24] were used to describe the electron core-valence interactions with the following configurations: La ($4f^0 5s^2 5p^6 5d^1 6s^2$), Ni ($3d^9 4s^1$), and O ($2s^2 2p^4$). A 550-eV plane-wave cutoff was used to obtain the ground state structure for each composition. Brillouin zone integrations employed the tetrahedron method [25], based on a Monkhorst-Pack k-point mesh obtained using the K-point grid server with 34 Å of minimum distance between lattice points [26,27]. The cell volume was relaxed and atomic positions were evolved until the forces on each atom were less than 1 meV Å^{-1}. We adopted the plus Hubbard U correction [28] of 1.5 eV for the correlated Ni $3d$ orbitals [5,29,30]. The effect of U on the formation energy and magnetic stabilities is discussed in the Supplementary Material (SM) [31].

Data from the literature describe the atomic structures of $LaNiO_{2.5}$ and $LaNiO_{2.75}$ as comprising OOVs in the [110] pseudocubic (pc) direction, forming NiO_6 and NiO_4 chains along the c axis as illustrated in Fig. 1 [32]. The inherently lower symmetry of the OOV phases compared to stoichiometric perovskites leads to higher complexity in potential distortion patterns. To efficiently survey the stable distortion patterns, we identified the rotation and tilting modes responsible for the two energy-competing space groups in $RNiO_3$: $a^-a^-a^-$ ($R\bar{3}c$) and $a^+a^-c^-$ ($Pnma$) [33]. The modes include (i) out-of-phase rotation ($a^-b^0b^0$), (ii) in-phase rotation ($a^+b^0b^0$), and (iii) tilting of apical oxygens ($a^0b^-b^-$). These modes were identified from ideal (nondistorted) structures using PHONOPY [34] and ISODISTORT [35,36].

When OOVs are introduced into $LaNiO_{3-\delta}$, the $LaNiO_{2.5}$ structure exhibits a checkerboard ordering of NiO_4 and NiO_6 columns on the $(001)_{pc}$ plane. Much less is known about the atomic structure of $LaNiO_{2.75}$ [37–39], which is conjectured to be an intermediate stoichiometric phase between $LaNiO_{2.5}$ and $LaNiO_3$. Based on the preference of vacancies to form square planar units [40] and diffraction peaks near the

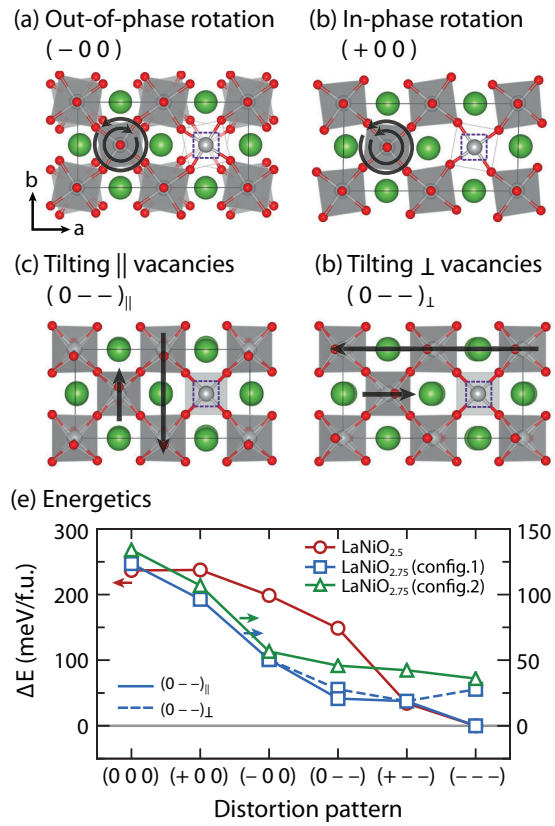

FIG. 2. Major distortion modes in [(a)–(d)] $LaNiO_{2.75}$ (config. 1): out-of-phase rotation, in-phase rotation, tilting of apical oxygen atoms parallel/perpendicular to the ordered vacancies. For $LaNiO_{2.5}$ and $LaNiO_{2.75}$ (config. 2), the two tilting modes are symmetrically identical. (e) Relative energies with different distortion patterns in $LaNiO_{3-\delta}$ phases with OOVs based on nonspin-polarized calculations.

boundary between $LaNiO_{2.5}$ and $LaNiO_3$ [10], we deduced that $LaNiO_{2.75}$ possesses fewer NiO_4 columns than $LaNiO_{2.5}$. The NiO_4 columns are replaced with columns of NiO_6 octahedra. This change in coordination led us to construct two distinct configurations (config. 1 and 2) for $LaNiO_{2.75}$. The configurations are distinguished by the *cis* or *trans* alignment of NiO_4 columns as illustrated in Figs. 1(c) and 1(d).

Adding OOVs to perovskite lowers the cubic symmetry to either tetragonal or orthorhombic: $P4/mmm$ ($LaNiO_{2.5}$), $Pmmm$ ($LaNiO_{2.75}$; config. 1), and $P4/mmm$ ($LaNiO_{2.75}$; config. 2). This anisotropic nature of OOV phases makes Glazer notation [41], which is used to describe octahedral rotations in perovskites relative to a set of Cartesian axes, not directly applicable. Here, we adopted a modified notation as follows: nondistorted (0), in-phase rotation (+), and out-of-phase rotations (−), as illustrated in Fig. 2. The orthorhombic parent structure of $LaNiO_{2.75}$ (config. 1) permits two different types of tilting modes about directions relative to the OOVs forming the NiO_4 units: $(0--)_{||}$ and $(0--)_{\perp}$ corresponding to the direction of apical oxygen tilting parallel (||) or perpendicular ($\perp$) to the NiO_4 layer, respectively, as shown in Figs. 2(c) and 2(d). The detailed group theoretical analysis of the tilt-symmetry breaking is described in the SM [31].

Figure 2 shows the general energetics for different distortions without magnetic interactions. For all phases, the out-of-phase $(0\ -\ -)$ tilting mode is more energetically favorable than either of the single in-phase or out-of-phase rotation modes. The lowest energy configurations are obtained by combination of either one of these single rotation modes, $(+\ 0\ 0)$ or $(-\ 0\ 0)$, with the tilting mode. Between the $(+\ -\ -)$ and $(-\ -\ -)$ patterns, we found the $(-\ -\ -)$ type pattern is lower in energy: 34.3 meV/f.u. for $LaNiO_{2.5}$, 18.7 meV/f.u. for $LaNiO_{2.75}$ (config. 1) and 6.34 meV/f.u. for $LaNiO_{2.75}$ (config. 2). For $LaNiO_{2.75}$ config. 1, the $(0\ -\ -)_{||}$ tilt is energetically prefered to the $(0\ -\ -)_{\perp}$ tilt, and it is more stable than config. 2 by 36 meV/f.u. This energy difference arises from the $(0\ -\ -)_{\perp}$ tilting, where oxygen atoms bridging square planar units are symmetrically locked along the vacancy plane direction (||). This locking makes it difficult to relax the strain induced by the oxygen vacancies, resulting in relatively higher energy.

Next, we study the effect of spin polarization on the energetics in Fig. 2. Although the relative energetics change, the overall trend is the same as that obtained from the nonspin-polarized calculations. Note that the stable reference spin configurations are A-AFM for $LaNiO_{2.5}$ and FM for $LaNiO_{2.75}$; a detailed discussion of these magnetic states is given further below. First, the energy difference between the $(+\ -\ -)$ and $(-\ -\ -)$ patterns is significantly reduced: 0.24 meV/f.u. for $LaNiO_{2.5}$, 9.8 meV/f.u. for $LaNiO_{2.75}$ (config. 1), and 2.8 meV/f.u. for $LaNiO_{2.75}$ (config. 2). In addition, the energy difference between configs. 1 and 2 is reduced further to less than 2 meV/f.u., indicating the strength of the magnetic interactions is comparable to the difference from elastic strain effects in the $(+\ -\ -)$ and $(-\ -\ -)$ octahedral patterns [31]. There is an approximate 10 % difference between the equatorial and apical Ni–O bond distances, regardless of the distortion patterns, in the octahedral units in OOV phases which presents like a compressed Jahn-Teller distortion; i.e., the equatorial bond length is longer than apical bond length. This distortion mainly originates from the significantly shorter Ni–O bond lengths in the NiO_4 units [32]. The bond length differences shift the bridging oxygen between the NiO_6 and NiO_4 closer to the NiO_4 unit, which elongates the octahedral unit in the *ab* plane. For $LaNiO_{2.75}$, a similar distortion is found within the larger octahedra whereas the smaller octahedra exhibit almost isotropic bond lengths (darker octahedra in Fig. 1). This Jahn-Teller-like distortion is distinguished from the conventional first-order Jahn-Teller distortion found in d^4 $LaMnO_3$, as the high-spin d^8 configuration within an octahedral crystal field lacks any orbital degeneracy, as discussed further below.

Our phonon calculations with spin-polarization confirmed the dynamic stabilities of the $(-\ -\ -)$ and $(+\ -\ -)$ patterns for $LaNiO_{2.5}$ and $LaNiO_{2.75}$ (config. 1) [31] with symmetries specified in Table I. The ground state $C2/c$ space group of $LaNiO_{2.5}$ agrees with the experimentally reported atomic structure [37–39]. In addition, we identified that the metastable structure with the $(+\ -\ -)$ tilt pattern and $P2_1/m$ space group is close in energy to the ground-state phase. Our phonon calculations for $LaNiO_{2.75}$ config. 1 further confirm that the $(-\ -\ -)_{\perp}$ tilt is dynamically unstable; any atomic perturbation drives the structure to relax into the $(-\ -\ -)_{||}$ tilt, which is then adopted and becomes the dynamically stable ground state ($P2/c$). Note that adding the $(+\ 0\ 0)$ mode to either $(0\ -\ -)_{\perp}$ or $(0\ -\ -)_{||}$ gives the same symmetry reduction, i.e., a $P2_1/m$ space group. This is not the case when adding the $(-\ 0\ 0)$ to those two-tilt systems. Although both $(-\ -\ -)_{\perp}$ and $(-\ -\ -)_{||}$ patterns exhibit the $P2/c$ space group, their tilting directions differ with respect to the vacancy plane. This difference leads to the $(-\ -\ -)_{||}$ pattern as the lowest energy and dynamically stable distortion (Table I). On the other hand, the in-phase rotation mode in config. 1 removes the symmetric difference between the two tilting modes, where single $(+\ -\ -)$-type pattern is obtained with the dynamically stable $P2_1/m$ space group. For config. 2 of $LaNiO_{2.75}$, both $(-\ -\ -)$ and $(+\ -\ -)$ distortions are dynamically unstable solutions. Modulating these two structures along the unstable distortions yields triclinic $P\bar{1}$ symmetry resembling the $(-\ -\ -)$ distortion, but with higher anisotropy of Ni-O bond lengths in the *ab* plane.

TABLE I. Summary of electronic and structural information of OOV $LaNiO_{3-\delta}$ phases. Electronic configuration of nickel atoms are provided based on polyhedral units, and space group of stable derivative OOV nickelates are listed. The structures of $LaNiO_{2.75}$ with config. 2 are dynamically unstable.

Features	$LaNiO_{2.5}$		$LaNiO_{2.75}$		
Polyhedra	Oct.	Square	Oct. (L)	Oct. (S)	Square
d-filling	d^8	d^8	d^8	d^6	d^8
Spin state	$S=1$	$S=0$	$S=1$	$S=0$	$S=0$

		$LaNiO_{2.75}$	
Tilt	$LaNiO_{2.5}$	config. 1	config. 2
$(+--)$	$P2_1/m$	$P2_1/m$	$P2_1/m$
$(---)$	$C2/c$	$P2/c$	$C2/c$

To identify the ground-state magnetic structure of $LaNiO_{2.5}$, we examined the energetic stabilities of different magnetic orders with the $(-\ -\ -)$ distortion that gives $C2/c$ symmetry. We found A-type AFM is the most stable and leads to an insulating gap of ≈0.75 eV (Fig. 3). The calculated magnetic moments are 1.5 μ_B and 0.15 μ_B for Ni^{2+} in the NiO_6 and NiO_4 units, respectively, which indicates each unit stabilizes high-spin (d^8, $S=1$) and low-spin (d^8, $S=0$) configurations. Our assignment of a low-spin configuration for the NiO_4 unit is also supported by its short Ni–O bond lengths of 1.88 Å that give a strong crystal field splitting effect [42]. The stability of A-type AFM order is consistent with the Goodenough-Kanamori-Anderson (GKA) superxchange rules for these orbital fillings [43,44]. As both e_g states of the octahedral unit are half-filled, the linear octahedral chains along c are AFM coupled to one another. The low-spin configuration on NiO_4 units are diamagnetic so their magnetic coupling is negligible. This leads to the small energy difference of 3.28 meV/f.u. between the A- and A^--type orders, where A^--AFM possesses both spin-up and spin-down octahedral units on the same *ab* plane as depicted in Fig. 3(a).

Our discussion of the magnetic structure of $LaNiO_{2.75}$ focuses on the monoclinic phase with config. 1 and the $(-\ -\ -)$ tilt distortion ($P2/c$). The ground state is a narrow gap insulator ($E_g \approx 0.1$ eV) with zigzag AFM order (E_a-AFM), as

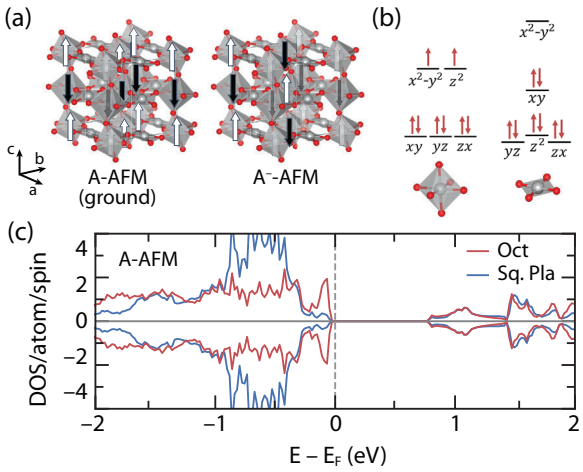

FIG. 3. (a) Stable magnetic orders in $LaNiO_{2.5}$. La atoms are omitted. (b) Electronic filling of the octahedral and square planar units. (c) Density of states (DOS) per Ni atom.

illustrated in Fig. 4. Although the orbital structure of the NiO_4 unit is similar to that in $LaNiO_{2.5}$, the Ni of the octahedral units in $LaNiO_{2.75}$ make the Ni states near E_F significantly more dispersive compared to insulating $LaNiO_{2.5}$. Interestingly, the band gap is sensitive to the magnetic order imposed. The zigzag spin order perpendicular to the vacancy plane (E_a) gives an insulating state whereas a zigzag spin order parallel to the vacancy plane (E_b) gives a metallic solution that is $\approx$6.6 meV/f.u. higher in energy than the insulating solution. The zigzag E-type order includes both FM and AFM coupling between large and small octahedral units, similar to magnetic solutions in the $RNiO_3$ family with rock-salt breathing distortions that support an insulating state [5]. In this regard, metallicity in $LaNiO_{2.75}$ may arise when either vacancy or magnetic order is disrupted. We also tested other zigzag magnetic orders (S- and T-AFM from Ref. [5]) and found energetically competing solutions; a quantitative comparison of magnetic stabilities and their U-value dependence is made in the SM [31].

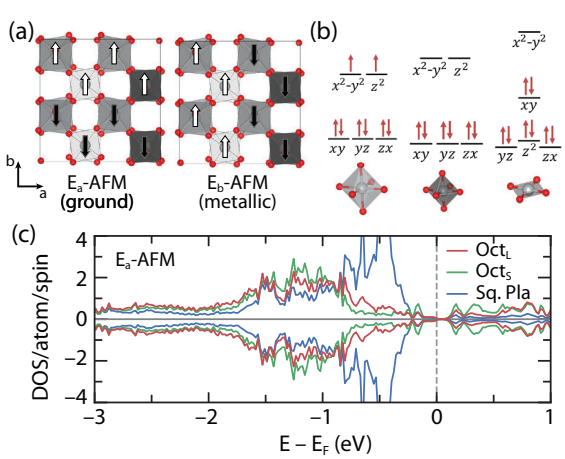

FIG. 4. (a) Stable magnetic orders in $LaNiO_{2.75}$. La atoms are omitted. (b) Electronic filling of the octahedral and square planar units. (c) Density of states (DOS) per Ni atom.

We found the E-type AFM is associated with columnar breathing distortion in $LaNiO_{2.75}$, which realizes charge ordering between large (light) and small (dark) octahedral units in Fig. 4. This behavior is not possible in $LaNiO_{2.5}$ owing to Ni^{2+} occupying both NiO_6 and NiO_4 units (Table I). The magnetic moments of the large and small octahedra are 1.2 μ_B and 0.7 μ_B, respectively, implying considerable charge disproportionation. Although the effective charge states are close to 2.5+ and 3+, they can be nominally assigned as Ni^{2+} and Ni^{4+} considering the significant degree of Ni–O hybridization, which agrees with ligand-associated charge ordering [45]. We attribute the origin of the columnar breathing distortion to the internal strain induced by the NiO_4 unit: The octahedral units on similar sites with NiO_4 units are subjected to compressive stresses to stabilize a similar level of bond valence with the NiO_4 units. The local Ni magnetic moment in the NiO_4 unit is 0.03 μ_B, which indicates the strong preference toward low-spin Ni^{2+} (d^8, $S = 0$). Thus, the breathing distortion is driven from stiff NiO_4 units in $LaNiO_{2.75}$. The charge ordering among Ni sites in the $LaNiO_{2.75}$ octahedra also occurs regardless of the metallic or magnetic order adopted.

The columnar arrangement of breathing distortion in $LaNiO_{2.75}$ is uniquely distinguished from that found in other $RNiO_3$ compounds. While rock-salt ordering of large and small octahedral units in $RNiO_3$ makes six connections for each octahedron to octahedral units of the other size, $LaNiO_{2.75}$ leaves connections between equivalent type of octahedra along the c axis with the number of smaller octahedra half the number of the larger units. With this unique arrangement, we also expect $LaNiO_{2.75}$ to possibly host novel phenomena with its unique electronic structure. First, a low-dimensional electron gas may be found above its MIT temperature when the narrow band gap is closed. Our DFT calculation predicts the metallic phase with AFM order is more stable than the FM spin order owing to the columnar breathing distortion. These AFM metals exhibit a low-dimensional electron gas, as shown in Fermi surface included in the SM [31], because electronic conduction is limited by the magnetic order and the NiO_4 planes. Second, the zigzag AFM order lifts inversion symmetry in the $P2/c$ space group, enabling multiferroic behavior in $LaNiO_{2.75}$. The polar magnetic space groups are P_b2_1 and Pc' for E_a- and E_b-AFM order, respectively, at the collinear-spin level, whereas noncollinear spins are required for multiferroicity in $LaNiO_3$ [46].

Coexistence of $LaNiO_{2.75}$ with perovskite $LaNiO_3$ may in part explain the unique behavior in $LaNiO_{3-\delta}$. For instance, a breathing distortion in $LaNiO_{3-\delta}$ was reported based on pair distribution (PDF) measurements [47]. The breathing distortion was attributed to the $P2_1/n$ space group like other low-temperature $RNiO_3$ structures, mainly because of the monoclinic feature appearing in the PDF data. The existence of $LaNiO_{2.75}$ was rejected despite the presence of oxygen vacancies because $LaNiO_{2.75}$ was previously reported as a triclinic rather than monoclinic structure [20]. Our work reveals that a monoclinic $LaNiO_{2.75}$ structure with columnar breathing distortion is energetically and dynamically stable, and its structure may better describe the local displacements observed experimentally in $LaNiO_{3-\delta}$. To discern the origin of the breathing distortions, we suggest analyses on the arrangement

of the smaller octahedral units or the relative proportion of octahedra with different sizes. Because of the 2:1 ratio of large to small octahedra, we expect different peak-height ratios in x-ray absorption spectra of $LaNiO_{2.75}$ compared to spectra of $RNiO_3$; furthermore, lower dimensional features may appear in angle-resolved photoemission spectra on single crystals of $LaNiO_{2.75}$ that could confirm its electronic description (see band structures in SM [31]).

Given our understanding now of the electronic structure of $LaNiO_{2.75}$, we now interpret the magnetic and electronic transitions found in $LaNiO_{3-\delta}$. Along the magnetic (PM-FM-AFM) and electronic (metal-semiconductor-insulator) transitions in the $LaNiO_{3-\delta}$ ($0 \leqslant \delta \leqslant 0.5$) series [13,14], the end-member phase $LaNiO_{2.5}$ best explains the AFM insulating state. On the other hand, the intemediate-member $LaNiO_{2.75}$ does not directly agree with the observed FM/semiconducting behavior. Noting that the ground state of $LaNiO_{2.75}$ is an AFM insulator with a narrow gap, we attribute the FM/semiconducting behavior to either a disruption of the vacancy order and/or disruption of the magnetic structure. When the structural vacancy order is imperfect, the formation of NiO_4 units reduces the number of states near E_F and inhibits electronic hopping, and clustered octahedral units would adopt either Ni^{2+} or Ni^{3+}, which spontaneously stabilizes FM spin coupling.

This view is supported by a $LaNiO_{2.75}$ report finding that the sign of $\partial\sigma/\partial T$ changes from semiconductor to correlated metal when thermally annealed [14], where considerable redistribution of oxygen vacancies is expected. However, we expect the formation of NiO_4 units are still preferred even when the vacancy order is disrupted as we find that config. 1 of $LaNiO_{2.75}$ is relatively more stable than other arrangements of oxygen vacancies, including the possibility of square pyramidal coordination (NiO_5 units) and randomly distributed vacancies, as discussed in the SM [31]. On the other hand, finite temperature might stabilize FM order over zigzag-type magnetic orders. The FM order is 16 meV/f.u. higher than the ground state [31], which may be thermally surmountable and could represent the FM feature observed in some $LaNiO_{3-\delta}$ crystals [10]. We additionally note that interfacial effects from $LaNiO_{2.75}/LaNiO_{2.5}$ or $LaNiO_{2.75}/LaNiO_3$ junctions may also play a role, especially because single-crystal $LaNiO_{2.75}$ has not been investigated without finite phase fractions of $LaNiO_{2.5}$ and $LaNiO_3$. Thus, we anticipate further experimental work dedicated to synthesis and property measurements of single-phase $LaNiO_{2.75}$ would help create a more complete view of topotactic transitions in $LaNiO_{3-\delta}$ and the range of phenomena accessible in complex nickelates.

We identified the detailed electronic and magnetic structure of oxygen-deficient $LaNiO_{3-\delta}$ with ordered oxygen vacancies. OOV in nickelate perovskites forms NiO_4 square planar units along the $(110)_{pc}$ plane, which stabilizes low-spin Ni^{2+} (d^8, $S = 0$) configuration. While these units become magnetically inactive, they tune the charge states of octahedral units which determine the magnetism of the OOV phases. For insulating $LaNiO_{2.5}$, the octahedral units exhibit high-spin Ni^{2+} (d^8, $S = 1$) and their structure along the c direction favors AFM coupling and stabilizes A-AFM order. The semiconducting $LaNiO_{2.75}$ phase exhibits a more complicated atomic structure comprising square planar units and dilated and/or contracted octahedral units. The columnar breathing distortion of octahedral units host charge disproportionation of Ni atoms to nominally Ni^{2+} and Ni^{4+} with zigzag-type AFM orders. The identified OOV phases can explain the electronic and magnetic properties with varying oxygen contents, and also contribute to the unique magnetic behavior of $LaNiO_{3-\delta}$ crystals.

Y.S. and J.M.R. acknowledge support from the National Science Foundation (NSF) under Award No. DMR-2011208. Calculations were performed using the QUEST HPC Facility at Northwestern, the Extreme Science and Engineering Discovery Environment (XSEDE), which is supported by the National Science Foundation under Grant No. ACI-1548562, and the Center for Nanoscale Materials (Carbon) Cluster, an Office of Science user facility supported by the U.S. Department of Energy, Office of Science, Office of Basic Energy Sciences, under Contract No. DE-AC02-06CH11357.

[1] J. B. Torrance, P. Lacorre, A. I. Nazzal, E. J. Ansaldo, and C. Niedermayer, Systematic study of insulator-metal transitions in perovskites $RNiO_3$ (R = Pr, Nd, Sm, Eu) due to closing of charge-transfer gap, Phys. Rev. B **45**, 8209 (1992).

[2] J. A. Alonso, J. L. García-Muñoz, M. T. Fernández-Díaz, M. A. G. Aranda, M. J. Martínez-Lope, and M. T. Casais, Charge disproportionation in $RNiO_3$ perovskites: Simultaneous Metal-Insulator and Structural Transition in $YNiO_3$, Phys. Rev. Lett. **82**, 3871 (1999).

[3] M. L. Medarde, Structural, magnetic, and electronic properties of R NiO_3 perovskites (R = rare earth), J. Phys.: Condens. Matter **9**, 1679 (1997).

[4] A. Mercy, J. Bieder, J. Íñiguez, and P. Ghosez, Structurally triggered metal-insulator transition in rare-earth nickelates, Nat. Commun. **8**, 1677 (2017).

[5] J. Varignon, M. N. Grisolia, J. Íñiguez, A. Barthélémy, and M. Bibes, Complete phase diagram of rare-earth nickelates from first principles, npj Quantum Mater. **2**, 21 (2017).

[6] N. Wagner, D. Puggioni, and J. M. Rondinelli, Learning from correlations based on local structure: Rare-earth nickelates revisited, J. Chem. Inf. Model. **58**, 2491 (2018).

[7] S. B. Lee, R. Chen, and L. Balents, Landau Theory of Charge and Spin Ordering in the Nickelates, Phys. Rev. Lett. **106**, 016405 (2011).

[8] S. B. Lee, R. Chen, and L. Balents, Metal-insulator transition in a two-band model for the perovskite nickelates, Phys. Rev. B **84**, 165119 (2011).

[9] J. Zhang, H. Zheng, Y. Ren, and J. F. Mitchell, High-pressure floating-zone growth of perovskite nickelate $LaNiO_3$ single crystals, Cryst. Growth Des. **17**, 2730 (2017).

[10] B.-X. Wang, S. Rosenkranz, X. Rui, J. Zhang, F. Ye, H. Zheng, R. F. Klie, J. F. Mitchell, and D. Phelan, Antiferromagnetic defect structure in $LaNiO_{3-\delta}$ single crystals, Phys. Rev. Materials **2**, 064404 (2018).

[11] K. Dey, W. Hergett, P. Telang, M. M. Abdel-Hafiez, and R. Klingeler, Magnetic properties of high-pressure optical

floating-zone grown $LaNiO_3$ single crystals, J. Cryst. Growth **524**, 125157 (2019).

[12] H. Guo, Z. W. Li, L. Zhao, Z. Hu, C. F. Chang, C.-Y. Kuo, W. Schmidt, A. Piovano, T. W. Pi, O. Sobolev, D. I. Khomskii, L. H. Tjeng, and A. C. Komarek, Antiferromagnetic correlations in the metallic strongly correlated transition metal oxide $LaNiO_3$, Nat. Commun. **9**, 43 (2018).

[13] T. Moriga, O. Usaka, I. Nakabayashi, T. Kinouchi, S. Kikkawa, and F. Kanamaru, Characterization of oxygen-deficient phases appearing in reduction of the perovskite-type $LaNiO_3$ to La_2 Ni_2 O_5, Solid State Ionics **79**, 252 (1995).

[14] R. D. Sánchez, M. T. Causa, A. Caneiro, A. Butera, M. Vallet-Regí, M. J. Sayagués, J. González-Calbet, F. García-Sanz, and J. Rivas, Metal-insulator transition in oxygen-deficient $LaNiO_{3-x}$ perovskites, Phys. Rev. B **54**, 16574 (1996).

[15] A. S. Botana and M. R. Norman, Similarities and Differences between $LaNiO_2$ and $CaCuO_2$ and Implications for Superconductivity, Phys. Rev. X **10**, 011024 (2020).

[16] D. Li, K. Lee, B. Y. Wang, M. Osada, S. Crossley, H. R. Lee, Y. Cui, Y. Hikita, and H. Y. Hwang, Superconductivity in an infinite-layer nickelate, Nature (London) **572**, 624 (2019).

[17] M. Kotiuga, Z. Zhang, J. Li, F. Rodolakis, H. Zhou, R. Sutarto, F. He, Q. Wang, Y. Sun, Y. Wang, N. A. Aghamiri, S. B. Hancock, L. P. Rokhinson, D. P. Landau, Y. Abate, J. W. Freeland, R. Comin, S. Ramanathan, and K. M. Rabe, Carrier localization in perovskite nickelates from oxygen vacancies, Proc. Natl. Acad. Sci. USA **116**, 21992 (2019).

[18] D. Misra and T. K. Kundu, Oxygen vacancy induced metal-insulator transition in $LaNiO_3$, Eur. Phys. J. B **89**, 4 (2016).

[19] X. Liao, V. Singh, and H. Park, Oxygen vacancy induced site-selective Mott transition in $LaNiO_3$, Phys. Rev. B **103**, 085110 (2021).

[20] J. M. González-Calbet, M. J. Sayagués, and M. Vallet-Regí, An electron diffraction study of new phases in the $LaNiO_{3-x}$ system, Solid State Ionics **32-33**, 721 (1989).

[21] G. Kresse and J. Furthmüller, Efficient iterative schemes for *ab initio* total-energy calculations using a plane-wave basis set, Phys. Rev. B **54**, 11169 (1996).

[22] G. Kresse and D. Joubert, From ultrasoft pseudopotentials to the projector augmented-wave method, Phys. Rev. B **59**, 1758 (1999).

[23] J. P. Perdew, K. Burke, and M. Ernzerhof, Generalized Gradient Approximation Made Simple, Phys. Rev. Lett. **77**, 3865 (1996).

[24] P. E. Blöchl, Projector augmented-wave method, Phys. Rev. B **50**, 17953 (1994).

[25] P. E. Blöchl, O. Jepsen, and O. K. Andersen, Improved tetrahedron method for Brillouin-zone integrations, Phys. Rev. B **49**, 16223 (1994).

[26] H. J. Monkhorst and J. D. Pack, Special points for Brillouin-zone integrations, Phys. Rev. B **13**, 5188 (1976).

[27] P. Wisesa, K. A. McGill, and T. Mueller, Efficient generation of generalized Monkhorst-Pack grids through the use of informatics, Phys. Rev. B **93**, 155109 (2016).

[28] S. L. Dudarev, G. A. Botton, S. Y. Savrasov, C. J. Humphreys, and A. P. Sutton, Electron-energy-loss spectra and the structural stability of nickel oxide: An LSDA + U study, Phys. Rev. B **57**, 1505 (1998).

[29] A. Hampel and C. Ederer, Interplay between breathing mode distortion and magnetic order in rare-earth nickelates $RNiO_3$ within DFT + U, Phys. Rev. B **96**, 165130 (2017).

[30] A. Hampel, P. Liu, C. Franchini, and C. Ederer, Energetics of the coupled electronic-structural transition in the rare-earth nickelates, npj Quantum Mater. **4**, 5 (2019).

[31] See Supplemental Material at http://link.aps.org/supplemental/10.1103/PhysRevResearch.4.L022069 for additional computational details including crystal structure information, phonon band structure, and density of states of other derivative structures.

[32] S. Estradé, F. Sánchez, G. Herranz, D. Pesquera, J. M. Rebled, N. Dix, M. J. Casanove, L. López-Conesa, C. Magén, J. Fontcuberta, and F. Peiró, Evidence of a minority monoclinic $LaNiO_{2.5}$ phase in lanthanum nickelate thin films, Phys. Chem. Chem. Phys. **19**, 9137 (2017).

[33] A. Subedi, Breathing distortions in the metallic, antiferromagnetic phase of $LaNiO_3$, SciPost Phys. **5**, 020 (2018).

[34] A. Togo, F. Oba, and I. Tanaka, First-principles calculations of the ferroelastic transition between rutile-type and $CaCl_2$-type SiO_2 at high pressures, Phys. Rev. B **78**, 134106 (2008).

[35] H. T. Stokes, D. M. Hatch, and B. J. Campbell, ISODISTORT, ISOTROPY Software Suite, iso.byu.edu.

[36] B. J. Campbell, H. T. Stokes, D. E. Tanner, and D. M. Hatch, ISODISPLACE: A web-based tool for exploring structural distortions, J. Appl. Crystallogr. **39**, 607 (2006).

[37] J. A. Alonso, M. J. MartinezLope, J. L. GarciaMunoz, and M. T. FernandezDiaz, A structural and magnetic study of the defect perovskite $LaNiO_{2.5}$ from high-resolution neutron diffraction data, J. Phys.: Condens. Matter **9**, 6417 (1997).

[38] J. A. J. A. Alonso, M. J. Martinez-lope, and M. J. Martínez-Lope, Preparation and crystal structure of the deficient perovskite $LaNiO_{2.5}$, solved from neutron powder diffraction data, J. Chem. Soc., Dalton Trans.,2819 (1995).

[39] T. Moriga, O. Usaka, T. Imamura, I. Nakabayashi, I. Matsubara, T. Kinouchi, S. Kikkawa, and F. Kanamaru, Synthesis, crystal structure, and properties of oxygen-deficient lanthanum nickelate $LaNiO_{3-x}$ ($0 \leqslant x \leqslant 0.5$), Bull. Chem. Soc. Jpn. **67**, 687 (1994).

[40] A. Malashevich and S. Ismail-Beigi, First-principles study of oxygen-deficient $LaNiO_3$ structures, Phys. Rev. B **92**, 144102 (2015).

[41] A. M. Glazer, The classification of tilted octahedra in perovskites, Acta Crystall. Sec. B **28**, 3384 (1972).

[42] Y. Matsumoto, T. Yamamoto, K. Nakano, H. Takatsu, T. Murakami, K. Hongo, R. Maezono, H. Ogino, D. Song, C. M. Brown, C. Tassel, and H. Kageyama, High-pressure synthesis of A_2 NiO_2 Ag_2 Se_2 (A = Sr, Ba) with a high-spin Ni^{2+} in square-planar coordination, Angew. Chem., Int. Ed. **58**, 756 (2019).

[43] J. B. Goodenough, *Magnetism and the Chemical Bond* (Interscience Publishers, John Wiley & Sons, 1963).

[44] J. Kanamori, Superexchange interaction and symmetry properties of electron orbitals, J. Phys. Chem. Solids **10**, 87 (1959).

[45] I. I. Mazin, D. I. Khomskii, R. Lengsdorf, J. A. Alonso, W. G. Marshall, R. M. Ibberson, A. Podlesnyak, M. J. Martínez-Lope, and M. M. Abd-Elmeguid, Charge Ordering as Alternative to Jahn-Teller Distortion, Phys. Rev. Lett. **98**, 176406 (2007).

[46] G. Giovannetti, S. Kumar, D. Khomskii, S. Picozzi, and J. van den Brink, Multiferroicity in Rare-Earth Nickelates R NiO_3, Phys. Rev. Lett. **103**, 156401 (2009).

[47] B. Li, D. Louca, S. Yano, L. G. Marshall, J. Zhou, and J. B. Goodenough, Insulating pockets in metallic $LaNiO_3$, Adv. Elect. Mat. **2**, 1500261 (2016).